

# On the Determination of the Deflection of the Vertical by Satellite Altimetry

A. B. Watts<sup>1</sup>  
K. Horai<sup>2</sup>  
N. M. Ribe<sup>3</sup>

Lamont-Doherty Geological Observatory  
Columbia University  
Palisades, New York

*Abstract* With the advent of satellite altimetry it has become possible to estimate the height of the marine geoid above the ellipsoid to an accuracy of better than 1 m. At a crossover of a satellite's ascending and descending tracks, altimeter data can be used to obtain two linearly independent estimates of the geoid's horizontal gradient. These two estimates determine the value of the deflection of the vertical at the crossover. We have used altimeter data obtained during the SEASAT mission to estimate deflections in an area of the Pacific Ocean in the vicinity of the Izu-Bonin and Mariana Trenches. The altimeter-derived deflections generally point outwards from the axis of the trench, reaching maximum amplitudes of up to 33 arc-sec over the walls of the trench. At a crossover of SEASAT's repeat tracks, altimeter data can be used to determine a number

Lamont-Doherty Geological Observatory Contribution Number 3582.

<sup>1</sup> Presently at: Meteorological College, Asahi-cho 7-4-81, Kashiwa-shi, Chiba-ken, Japan 277.

<sup>2</sup> Also at Department of Geological Sciences of Columbia University, New York, NY.

<sup>3</sup> Presently at Yale University, New Haven, CT.

*Marine Geodesy*, Volume 8, Numbers 1-4

0149-0419/84/010085-00\$02.00/0

Copyright © 1984 Crane, Russak & Company, Inc.

of estimates of the deflection at approximately the same point. The mean root mean square (RMS) difference in the magnitude and direction of the deflection at 13 intersections of SEASAT's repeat tracks are  $\pm 1.9$  arc-sec and  $\pm 14.9^\circ$ , respectively. We attribute these variations to instrument noise and oceanic variability. Deflections have also been estimated in two other regions of the Pacific Ocean by using altimeter data: one in the region of the Magellan Seamounts and one in the region of the Line Islands. In general, deflections are largest (up to 25 arc-sec) in the region of the Magellan Seamounts and smallest (up to 10 arc-sec) in the region of the Line Islands. We attribute these variations to formation of the Magellan Seamounts on older, stronger, oceanic lithosphere than the Line Islands.

## **Introduction**

The deflection of the vertical is an angle between two vectors: one normal to the local geoid and the other to the reference ellipsoid. On the earth's surface, astronomically determined positions are referred to the geoid, whereas geodetically derived positions are based on the reference ellipsoid. Thus, differences in astronomic and geodetic positions determine the deflection of the vertical. The deflection of the vertical has proved useful in representing the earth's gravity field in geophysical, geological, and geodetic studies.

One of the earliest uses of the deflection of the vertical was in the formulation of models to describe the compensation of the earth's topography. In 1842, for example, G. Everest calculated the differences between astronomic and geodetic positions in northern India, and found significant differences as the foothills of the Himalayas were approached. Everest (1842) attributed these discrepancies to uncertainties in the geodetic positions, since these were based on measurements of distances and angles between points on the earth's physical surface and an assumed flattening for the best fitting reference ellipsoid. Pratt (1855), however, argued that it was not the geodetic positions that were in error, but the astronomic positions, since the latter were referred to the geoid. He pointed out that in northern India the geoid is locally perturbed by the gravitational attraction of the

Himalayas and Tien Shan to the north. He calculated the effect of the mountains on the deflection of the vertical in northern India, assuming a uniform density for the terrain above sea level, and found that the Himalayas and Tien Shan would cause a deflection of the vertical of about 15 arc-sec. more than three times the measured value. Airy (1855) interpreted this discrepancy as the consequence of a low-density region below the mountain that competed with the gravity effect of the mountain itself. A controversy then developed as to the form of the low-density region: Airy (1855) proposed lateral changes in the thickness of a uniform-density crustal "root," while Pratt (1858) suggested lateral changes in the density of a crustal and upper mantle layer of uniform thickness. It was argued in both models, however, that pressures were equal at some depth (the depth of compensation) and that the outer layers of the earth would be in equilibrium unless disturbed by erosion and sedimentation. This tendency of the earth's surface to approach gravitational equilibrium was termed *isostasy* by Dutton (1882).

The deflection of the vertical had a more practical use in mapping and surveying, however. The usual approach in geodetic surveys is triangulation from a point whose position is known from astronomic techniques. It was found in the earliest surveys that significant closure errors occurred between adjoining surveys which could only be attributed to the astronomic positions. Thus, to establish a national network of precise geodetic positions, the astronomical positions required correction for the effects of local deflections of the vertical, a task which fell in the United States in 1909 to J. F. Hayford, the first director of the U.S. Coast and Geodetic service.

The initial approach adopted by Hayford was to compute the deflection of the vertical at an astronomic position from the surrounding topography and its compensation. The problem with this method was that it required an assumption for the form of isostatic compensation of the topography. In the United States, the Pratt model of isostasy was generally adopted. However, this model could not be verified at the time by seismic refraction and reflection data.

Subsequently, methods were developed to compute the de-

flexion of the vertical directly from a horizontal distribution of gravity anomalies (e.g., Rice, 1952; Heiskanen and Vening Meinesz, 1958; Nagy, 1963). Rice (1952), for example, used 40,000 gravity anomaly values from the south-central United States, each value having a precision of about 0.3 mgal. He included gravity data out to a radius of 500 km and calculated deflections that were precise to about 0.1 arc-sec. At the astronomic positions, Rice (1952) found close agreement between computed and measured deflections.

Although the deflection of the vertical can be accurately estimated on land, it has been more difficult to determine at sea. One of the first attempts was made by von Arx (1966), who measured differences in astronomic and geodetic positions on a ship crossing of the east-west trending Puerto Rico trench. He used a GEON system to estimate astronomic positions and LORAN-C to determine geodetic positions. The Puerto Rico trench was crossed in a north-south direction in order to obtain a reliable estimate of the total deflection. Von Arx (1966) determined deflections over the trench that ranged in amplitude from 60 to 90 arc-sec, finding qualitative agreement with deflections computed from gravity anomaly data measured along the same profile. Because of poor navigational control, however, deflections could not be determined by this method with a precision better than about 12 arc-sec.

Since the study by von Arx (1966), numerous gravity measurements have been obtained in the world's oceans by government and university research groups. But it is still not possible to use gravity measurements to compute deflections at sea with the same precision as on land. Gravity measurements at sea need to be corrected for the heave, surge, and sway of the ship, as well as for speed and heading variations. In general, measurements made at sea are less precise than those taken on land by an order of magnitude or more. However, in regions of closely spaced ship tracks, such as the western North Atlantic, it has been possible to compute gravimetric geoids with a horizontal resolution of 100 km and a vertical resolution of 50 cm (Marsh and Chang, 1978), implying deflections precise to about 1 arc-sec.

In regions of sparse gravity data, workers at the Defense Mapping Agency have used bathymetric data to estimate the value of the deflection of the vertical at sea. Deflections have now been computed over a variety of geological features, including seamounts, oceanic islands, and midocean ridge crests. Typically, deflections reach 15 arc-sec at midocean ridge crests (Fischer, 1979) and 25 arc-sec at seamounts and oceanic islands (Fischer and Wyatt, 1974). By comparing computed deflections based on bathymetry with measured astrogeodetic deflections on oceanic islands, Fischer and Wyatt (1974) concluded that deflections could be computed from bathymetry data to an accuracy of about 3 arc-sec.

To compute the deflection of the vertical accurately from bathymetry data, however, it is first necessary to assume some model of isostatic compensation for the bathymetry. In her studies, Fischer ignored isostasy by assuming that all bathymetry (except the broad flanks of midoceanic ridges) was uncompensated.

A number of studies have now shown that the amplitude and wavelength of gravity and geoid anomalies over bathymetric features are a strong function of their tectonic setting (e.g., Watts et al., 1980). For example, seamounts that form on young oceanic lithosphere, on or near a midocean ridge crest, are more locally compensated and are associated with low-amplitude, short-wavelength gravity and geoid anomalies, whereas seamounts that form on old lithosphere, off-ridge, are more regionally compensated and are associated with relatively high-amplitude, long-wavelength anomalies. These differences in gravity and geoid anomalies have been interpreted as a consequence of the increasing rigidity of the oceanic lithosphere as it cools away from the ridge crest. Since the deflection of the vertical is determined from the horizontal distribution of gravity and geoid anomalies, we would expect significant differences in its magnitude over seamounts formed on or near a ridge crest and off-ridge.

The gravity and geoid anomalies over seamounts are also dependent on the details of the isostatic model that is assumed (e.g., Watts and Ribe, 1983). For example, the geoid anomaly over a seamount formed on a 80 m.y. continuous elastic plate differs in amplitude and wavelength from that of a seamount formed on

a similarly aged fractured plate. The differences in the amount of flexure predicted by these models, however, is mainly limited to the region immediately underlying the seamount load, so that the slope of the geoid anomalies for the two cases is generally similar. Thus, it would not be expected that the deflection of the vertical would vary significantly between different isostatic models.

These considerations suggest that if the deflection of the vertical can be determined at sea it may provide useful information on the state of isostasy of bathymetric features in the world's ocean basins.

With the development of satellite altimetry during the past few years it has become possible to estimate the slope of the marine geoid on a global basis. Satellite altimeters directly measure the distance between a satellite and the instantaneous sea surface. By accurately determining the satellite orbit with respect to positions on the earth's surface, it is possible to estimate the height of the sea surface above the reference ellipsoid. The height of the sea surface corresponds closely to the marine geoid.

The deflection of the vertical is the angle between two vectors: one normal to the local geoid and one to the reference ellipsoid (see Figure 1). Since satellite altimetry enables the geoid height above a reference ellipsoid to be estimated, it can be used to estimate deflections at sea. Brammer (1979), for example, used GEOS-3 altimeter data to compute deflections over the western North Atlantic. By comparing the altimetric deflections to deflections computed from unpublished U.S. Navy gravity data, he estimated that the relative accuracy of the altimetric deflections was in the range from 2 to 5 arc-sec. More recently, Sandwell (1984) used SEASAT altimeter data to compute deflections over the southwest Pacific. Both studies, however, computed deflections along individual satellite altimeter tracks. Thus, Brammer (1979) and Sandwell (1984) determined components of the deflection rather than its total value.

We describe in this paper a method for computing the deflection of the vertical at crossover points of satellite altimeter data. The method is applied to the SEASAT data set over a test area of the Izu-Bonin and Mariana trenches, where a large amount of data on free-air gravity anomalies and bathymetry have al-

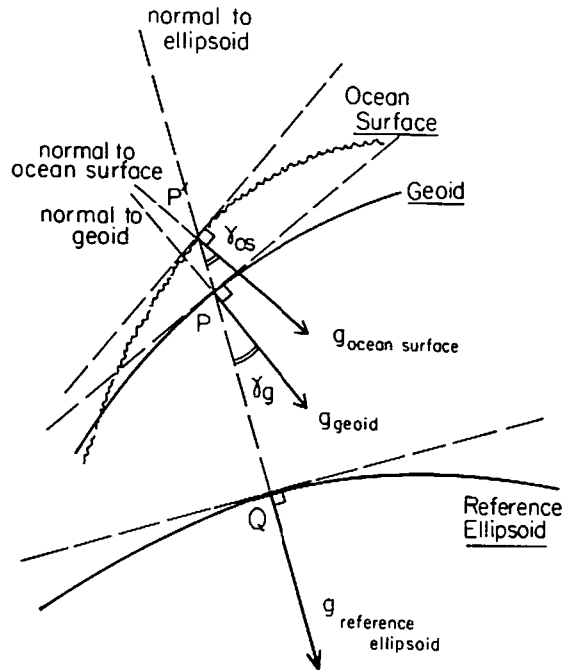


FIGURE 1. The geometry of the deflection of the vertical at sea. The arrows indicate the normals to the reference ellipsoid, geoid, and ocean surface. The deflections of the vertical corresponding to the geoid and ocean surface are indicated by  $\gamma_g$  and  $\gamma_{os}$ , respectively. The ocean surface shown may not correspond to the actual ocean surface, because geostrophic flow may contribute to changes in the sea-surface slope but not the deflection of the vertical.

ready been collected by surface ships. By qualitatively comparing the deflections determined from altimeter data with deflections predicted by existing gravity and bathymetry data, we conclude that satellite altimetry provides a reliable method for estimating deflections at sea. We briefly examine in this paper the implications of these results for tectonic studies of the world's ocean basins.

### Method

The use of radar altimeters on orbiting satellites to measure sea-surface heights has been discussed now for more than a decade. However, results useful for geological and geophysical studies

were not produced until recently (e.g., Leitao and McGoogan, 1975), using data from the Skylab and GEOS-3 satellites. The relative accuracy of the altimeter data, as indicated by analysis of sea-surface height discrepancies at intersecting satellite tracks, is in the range  $\pm 80$  to  $\pm 120$  cm for Skylab (Leitao and McGoogan, 1975) and  $\pm 20$  to  $\pm 60$  cm for GEOS-3 (Rapp, 1979). The noise levels associated with these altimeters was greatly reduced in the data obtained during the SEASAT mission. For example, Tapley et al. (1982) and Brammer and Sailor (1980) have estimated that noise levels for SEASAT are better than  $\pm 10$  cm, making the data useful for geological and geophysical studies as well as for studies of the oceanic variability.

The SEASAT satellite was launched on June 28, 1978 into a nearly circular orbit at an inclination angle of  $108^\circ$ . Any forty-three consecutive revolutions of SEASAT produced global coverage (Schutz et al., 1982). Because of the earth's ellipticity and rotation, nonconsecutive revolutions crossover at intervals of about  $9.4^\circ$  at the equator. The satellite failed after 106 days, however, allowing thirty-five sets of three-day global coverage to be completed. Since three-day global coverage effectively drifts  $1^\circ$  to  $2^\circ$  for each period of three days, the differences in longitude of nonconsecutive crossover points does not exceed  $2^\circ$  and is usually closer to  $1^\circ$ . In the last month of the mission, the three-day coverage virtually did not drift at all, so that differences in the longitude of crossover points does not exceed  $0.015^\circ$ . The average number of usable crossovers for each three-day interval during the mission is about 900, giving a total number of crossovers for the entire mission of about 322,200.

At a crossover point, profiles of the measured sea-surface height give two linearly independent estimates of the geoid's horizontal gradient: one along the satellite's ascending track and one along its descending track. These two estimates of the geoid's horizontal gradient determine the direction of the geoid's vertical (Figure 1). Since individual estimates of the sea-surface height on either side of a crossover point are referred to the ellipsoid, the direction of the geoid's vertical determines the local deflection of the vertical.

We illustrate this by introducing a local Cartesian coordinate

system with its origin coinciding with the geographical coordinates of the crossover ( $\phi_c, \lambda_c$ ) and its  $xy$  plane tangential to the reference ellipsoid (Figure 2). Since altimeter data consist of a set of discrete values of the sea-surface height measured along a satellite's track, the geoid's horizontal gradient vector along the ascending track,  $\mathbf{A} = (x_a, y_a, z_a)$ , is given in this coordinate system by

$$\begin{aligned} x_a &= C_x(x_{a2} - x_{a1}) \\ y_a &= C_y(y_{a2} - y_{a1}) \\ z_a &= h_{a2} - h_{a1} \end{aligned} \quad (1)$$

where  $(x_{a2}, y_{a2}, h_{a2})$  and  $(x_{a1}, y_{a1}, h_{a1})$  are two ascending data points on either side of the crossover point and  $C_x = (\pi/180)R$

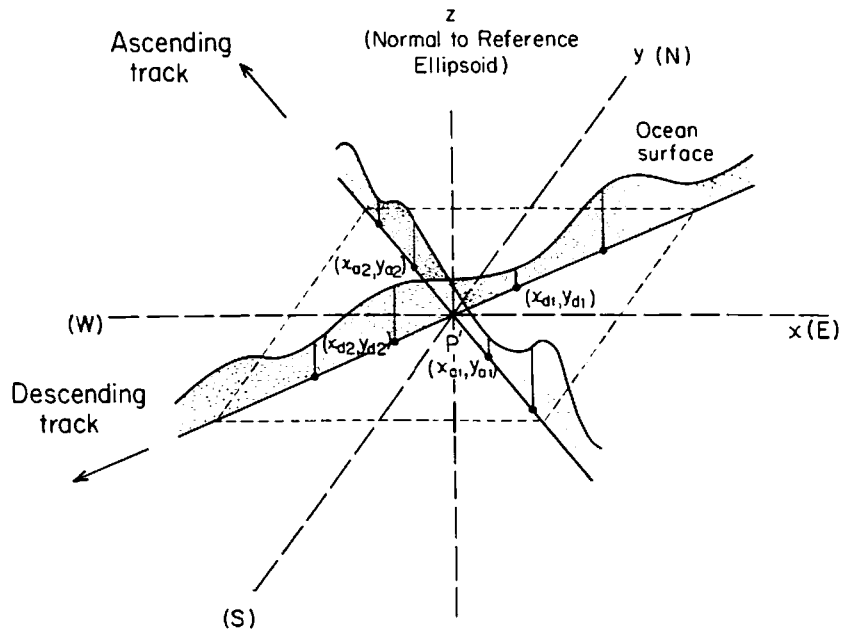


FIGURE 2. Schematic diagram of the coordinate system used in this paper. The origin  $P'$  coincides with the crossover position of a satellite's ascending and descending tracks.

and  $C_y = (\pi/180)R \cos(\phi_c)$  are conversion factors of the geographical coordinates of a spherical earth of radius  $R$  into the local coordinate system. Similarly, the geoid's horizontal gradient vector along the descending track,  $\mathbf{D} = (x_d, y_d, z_d)$ , is given by

$$\begin{aligned}x_d &= C_x(x_{d2} - x_{d1}) \\y_d &= C_y(y_{d2} - y_{d1}) \\z_d &= h_{d2} - h_{d1}\end{aligned}\quad (2)$$

The direction of the geoid's local vertical at the crossover point is normal to both  $\mathbf{A}$  and  $\mathbf{D}$ . Thus we can define a unit vector  $\mathbf{U}$  by

$$\mathbf{U} = -(\mathbf{A} \times \mathbf{D})/|\mathbf{A} \times \mathbf{D}| \quad (3)$$

The components of  $\mathbf{U}$ , pointing downward, are (Figure 3):

$$\begin{aligned}U_x &= -(y_a z_d - y_d z_a)/U \\U_y &= -(z_a x_d - z_d x_a)/U \\U_z &= -(x_a y_d - x_d y_a)/U\end{aligned}\quad (4)$$

Thus

$$U = [(y_a z_d - y_d z_a)^2 + (z_a x_d - z_d x_a)^2 + (x_a y_d - x_d y_a)^2]^{1/2} \quad (5)$$

Because the values of sea-surface height ( $h_{a1}$ ,  $h_{a2}$ ,  $h_{d1}$ ,  $h_{d2}$ ) are referred to the ellipsoid, the angle  $\gamma$  between  $\mathbf{U}$  and the  $z$ -axis of the local Cartesian coordinate system

$$\gamma = \tan^{-1}[U_z/\sqrt{(U_x^2 + U_y^2)}] \quad (6)$$

defines the deflection of the vertical. The azimuth of the de-

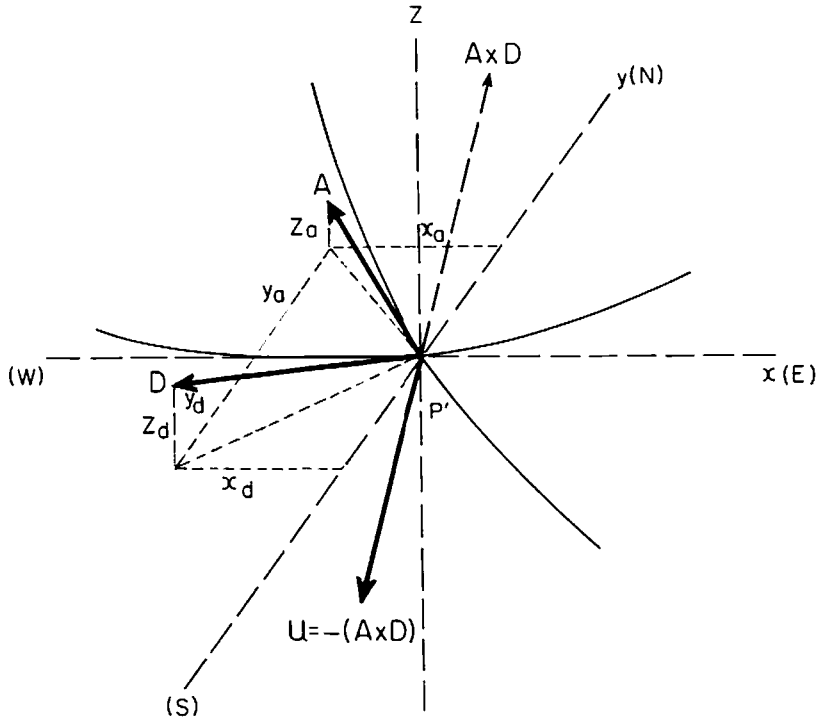


FIGURE 3. Vector diagram at the crossover of a satellite's ascending and descending tracks. *A* is the horizontal gradient of the sea surface along the ascending track and *D* is the gradient along the descending track.

Deflection of the vertical with respect to the *y*-axis of the local coordinate system is then

$$\alpha = \tan^{-1}(U_x/U_y) \quad (7)$$

We have assumed in this discussion that the sea-surface height measured by a satellite altimeter closely approximates the marine geoid. In practice, however, instrument noise and oceanic variability may also contribute to variations in the sea-surface height. Thus the deflection of the vertical derived from altimeter data may include components that are due to gravity as well as to instrument noise and oceanic variability.

## Results

We have applied the method discussed in the previous section to SEASAT altimeter data from a test area over the Izu-Bonin and Mariana trenches in the western Pacific Ocean. This region was selected because the gravity anomaly, bathymetry, and geoid have already been mapped in the region (Chase et al., 1971; Watts, 1976; Horai, 1982). Further, the region is associated with high-amplitude<sup>4</sup> gravity and geoid anomalies and includes the linear Izu-Bonin and Mariana deep-sea trench island-arc systems.

The SEASAT data used in this paper represent sea-surface heights measured above the reference ellipsoid. The data comprise 1-s averages and have been corrected for instrument and atmospheric effects, as described in the Jet Propulsion Laboratory (JPL) SEASAT data users' handbook (Lorell et al., 1980). We did not correct the SEASAT data for oceanic variability resulting from oceanographic, tidal, or meteorological effects. Further, no attempt was made to reduce sea-surface height discrepancies at individual crossover points. Typically, these discrepancies are in the range  $\pm 1$  to  $\pm 2$  m for SEASAT data and result mainly from errors in the determination of the orbit of the satellite. The orbit error for periods of one-quarter of a revolution of SEASAT is about 150 cm, corresponding to an error in the geoid's horizontal gradient (and the deflection of the vertical) of only about 0.03 arc-sec. Thus, by considering the slope of the geoid, rather than its absolute height, the effect of orbit errors are substantially reduced.

Figure 4 summarizes the estimates of the deflection of the vertical for the test area of the Izu-Bonin and Mariana deep-sea trenches. For simplicity, only deflections determined in the immediate vicinity of trench are shown in the figure. Figure 4a shows the locations of the deflections and Figure 4b illustrates their magnitude and direction. A summary of the track identification, geoid heights, and deflections at each crossover is given

<sup>4</sup> The free-air gravity anomaly of +397.1 mgal measured during R/V Vema cruise 21 leg 7 at latitude 27.983°N and longitude 141.948°E is to our knowledge the largest recorded in oceanic regions.

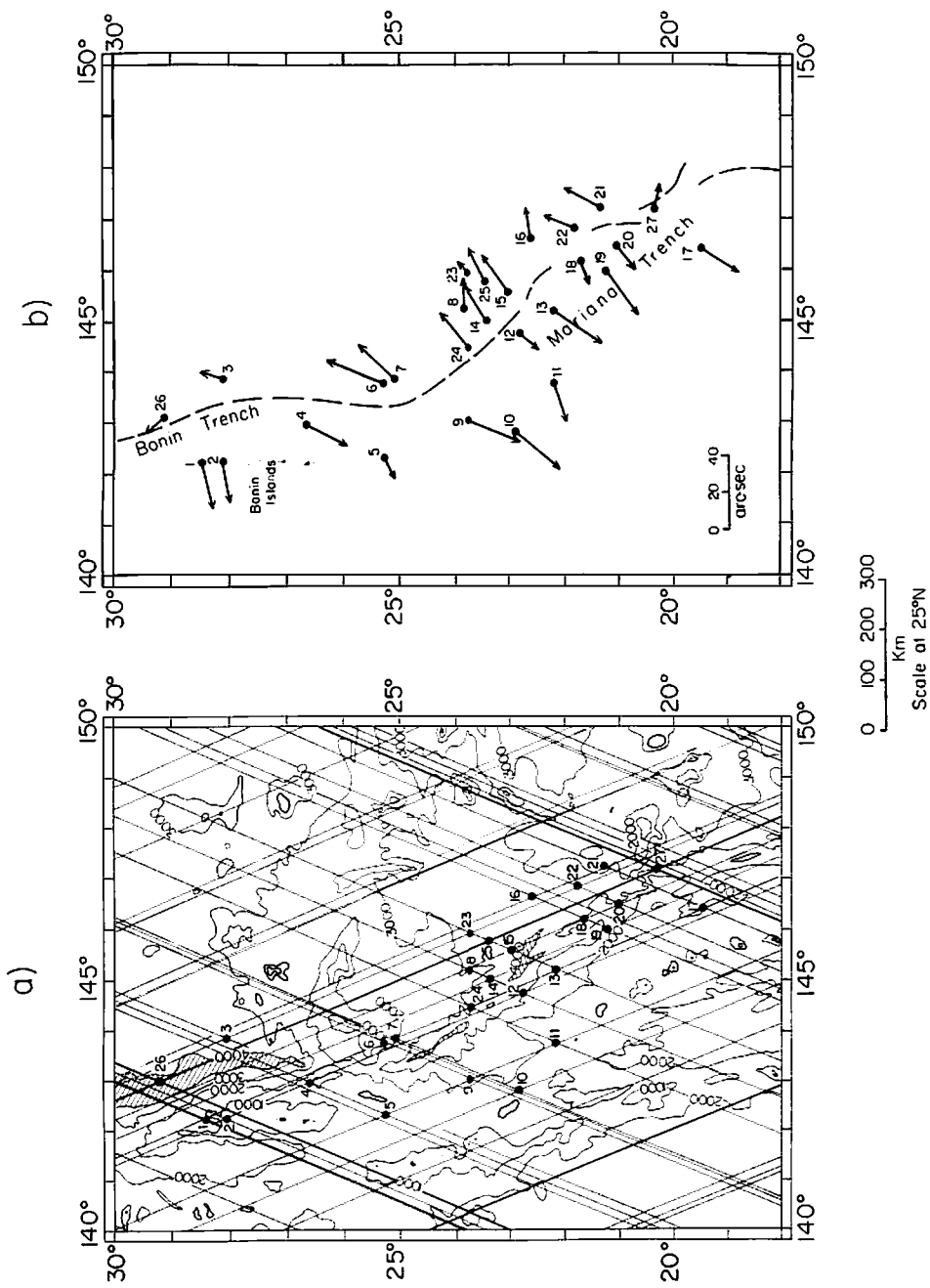
in Table 1. The deflections in Figure 4*b* were computed from the actual value of the sea-surface height on either side of the cross-over point of an ascending and descending track.

There is generally good agreement between the direction of the altimeter-derived deflections and large-scale bathymetric trends in the test area (Figure 4*b*). In general, deflections point outwards, away from the trench axis, in a direction normal to the local trend of the trench. This pattern of deflections is consistent with the trench representing a region of mass deficiency compared to adjacent island arc and outer rise regions. The main exceptions are estimates 3, 26, 6, and 4, which are oriented at a relatively high angle to the local normal to the trench. In the case of estimates 4 and 6, however, this probably results from local bathymetric irregularities in the trend of the landward and seaward walls of the trench respectively.

The magnitude of the deflections in Figure 4 range from 8.6 to 33.6 arc-sec, with the greatest values occurring over the maximum change in the slope of the landward and seaward walls of the trench. The deflections are generally small over the trench axis itself and in regions flanking the trench and island arc system.

The altimeter-derived deflections are unlikely to correlate precisely with bathymetry because of isostasy. Studies of the relationship between free-air gravity anomalies and bathymetry in the world's oceans (e.g., McKenzie and Bowin, 1976) show that at short wavelengths a strong correlation exists between gravity and bathymetry, but that at long wavelengths the correlation decreases until there is little or no correlation. This dependence of the gravity anomaly on wavelength occurs because short-wavelength bathymetric features are uncompensated, whereas long-wavelength features are compensated. Since the deflection of the vertical is determined by the horizontal distribution of the gravity anomalies, we would expect large deflections over uncompensated features and small deflections over compensated features. Thus depending on the wavelength, deflections may not correlate closely with the bathymetry.

We compare the altimeter-derived deflections to a free-air gravity anomaly map of the test area in Figure 5. The map is



contoured at 25-mgal intervals and incorporates all surface-ship data that were collected in the region before 1975 (Watts, 1976). Figure 5 shows there is generally a good correlation between the deflections and the main features of the gravity anomaly map. In particular, estimates 1, 2, 6, 7, 10–15, 18–20, and 23–25 are generally oriented normal to the local gravity gradients. The main exceptions are estimates 3–5, 8, 9, 16, 17, 21, and 22, which are oriented at relatively high angles to the local gravity gradients. Figure 5 shows, however, that most of these estimates occur between individual ship tracks where gravity data are sparse. In the case of estimate 6, a nearby surface ship track shows there is a gravity anomaly high seaward of the trench wall that is apparently large enough to reorient the local deflection of the vertical toward it and away from a direction normal to the trench axis.

It is possible, as Rice (1952) and others have shown, to compute the deflection of the vertical from the horizontal distribution of gravity anomalies and compare it directly to observed deflections. The calculation of deflections from gravity data, however, requires detailed knowledge of the near-field gravity anomaly around a point of interest. Rice (1952), for example, argued that in order to achieve an accuracy of 1 arc-sec or better it is necessary to have knowledge of the gravity field out to a radius of at least 200 km. Clearly, the gravity data in Figure 5 are not suitable for such a calculation because of the paucity of surface-ship measurements. In general, only one or two ship tracks cross a 1° by 1° “square.” Further, there are some “squares” in the trench region for which there are no measurements at all.

---

←  
**FIGURE 4.** SEASAT altimeter tracks, bathymetry, and deflections of the vertical in the vicinity of the Izu-Bonin and Mariana deep-sea trench. The heavy dots in *a* indicate the location of the deflections in *b*. The dashed line in *b* indicates the approximate position of the greatest trench depths, obtained by tracing the minimum of the 4000-fathom contour (1 fathom = 1.8288 m). The length of the arrows in *b* gives the magnitude of the deflection; the direction of the arrows corresponds to the direction of the deflection. The deflections decrease in magnitude as the trench axis is approached and generally point outwards, away from the trench axis, in a direction normal to the local strike of the trench.

**Table 1**  
Crossover Analysis at Intersections 1 Through 24 (Figure 4)

Crossover	Ascending Track	Descending Track	Geoid Height		Position of Crossover		Deflection of Vertical	
			Ascending, cm	Descending, cm	Latitude, °N	Longitude, °E	Azimuth, degrees	Magnitude, arc-sec
1	2019	2154	4655.1	4776.5	28.44	142.22	243.4	28.1
2	3211	617	5038.4	5211.7	28.10	143.22	259.2	22.7
3	2280	455	2882.6	3103.0	28.09	143.84	17.6	9.6
4	3211	879	3801.8	3862.2	26.63	142.94	207.4	24.5
5	1749	879	4067.7	4273.7	25.29	142.30	239.6	12.8
6	2019	1149	3990.9	4099.4	25.29	143.75	22.2	32.4
7	2019	2630	3901.2	3903.9	25.17	143.81	42.5	33.3
8	3475	2903	3773.3	3723.0	23.80	145.21	91.6	18.5
9	1749	1149	3478.7	3765.8	23.75	143.03	292.0	32.5
10	2940	2630	4403.1	4475.6	22.93	142.76	221.8	31.5

11	1749	1434	4249.0	4455.1	22.18	143.75	251.9	20.1
12	3211	2903	2835.4	2919.9	22.79	144.75	218.7	14.6
13	2019	1713	3047.2	3194.5	22.18	145.19	214.4	31.4
14	54	2903	3158.0	3268.5	23.88	145.02	58.1	21.8
15	3475	1713	3182.2	3209.8	23.01	145.58	56.0	23.9
16	739	3168	3405.0	3357.6	22.60	146.62	92.3	15.3
17	2019	3431	3870.8	3736.8	19.47	146.41	212.2	22.9
18	3475	3168	3025.0	2867.3	21.66	146.19	247.4	12.5
19	54	3168	3315.6	3302.0	21.23	145.99	233.3	29.7
20	3475	12	3338.7	3237.9	21.02	146.48	228.6	15.5
21	739	3431	3378.4	3171.5	21.29	147.21	28.1	20.2
22	2280	12	2898.0	3144.3	21.78	146.82	20.6	17.0
23	2280	1713	3568.5	3923.4	23.75	145.92	52.8	8.6
24	2019	1434	3245.1	3273.7	23.75	144.47	49.7	24.7

<sup>a</sup> Note that the track identification used in this paper differs from that used on the JPL data tapes. Individual tracks are plotted in Figure 4.

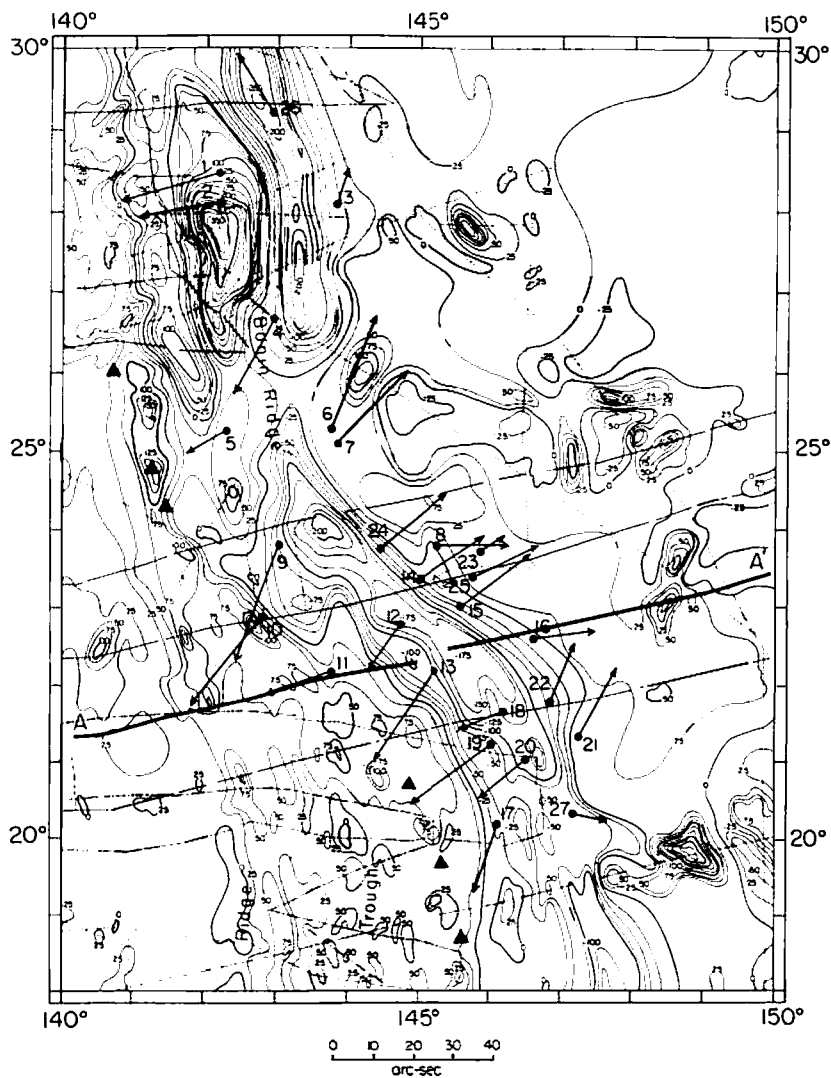


**FIGURE 5.** The deflection of the vertical in the vicinity of the Izu-Bonin and Mariana trenches superimposed on a free-air gravity anomaly map of the region contoured at 25-mgal intervals. The fine dots indicate the location of individual free-air gravity anomaly values used to construct the gravity anomaly map (Watts, 1976). The heavy dots indicate the location of the deflections of the vertical in Figure 4a. The heavy continuous line shows the location of the free-air gravity anomaly and topography in Figure 6.

We therefore compare the deflections of the vertical determined from altimeter data at estimates 11 and 16 (Figure 4*b*, Figure 5) to calculated values based on gravity anomaly data measured along a single ship track over the Mariana trench. Profile AA' was selected for the comparison because it is within 15 km of and is generally parallel to the deflections at estimates 11 and 16. We assumed in the calculations that the local gravity field is two-dimensional and extends in a direction normal to the ship track. Assuming a flat earth, the geoid anomaly associated with a gravity anomaly can be expressed as

$$H(k) = G(k)/gk \quad (8)$$

where  $H(k)$  is the geoid anomaly in the wave number domain,  $G(k)$  is the gravity anomaly in the wave number domain,  $k$  is the wave number that is related to the anomaly wavelength  $\lambda$  by  $k = 2\pi/\lambda$ , and  $g$  is the average gravity. (The geoid anomaly in the space domain is  $h(x)$ , and  $g(x)$  is the gravity anomaly in the space domain.) The deflection of the vertical is given by the gradient of the geoid, namely

$$\gamma(x) = (d/dx)h(x) \quad (9)$$

Rewriting in the wave number domain yields

$$\gamma(k) = ikH(k) \quad (10)$$

We used Equations (8) and (10) to compute the geoid and deflection of the vertical profiles in Figure 6.

There is good qualitative agreement in Figure 6 between the deflections calculated from the gravity anomaly and those determined from altimeter data. Quantitatively, however, the deflections differ by as much as 10% to 20%. The closest agreement is for estimate 11, where the strike of the local gravity anomaly gradient is generally normal to the ship track. Estimate 16, on the other hand, shows the largest disagreement, probably because the local gravity gradient strikes at a high angle to the normal to the ship track (Figure 5).

The deflection estimates in Figures 4 and 5 are mainly based

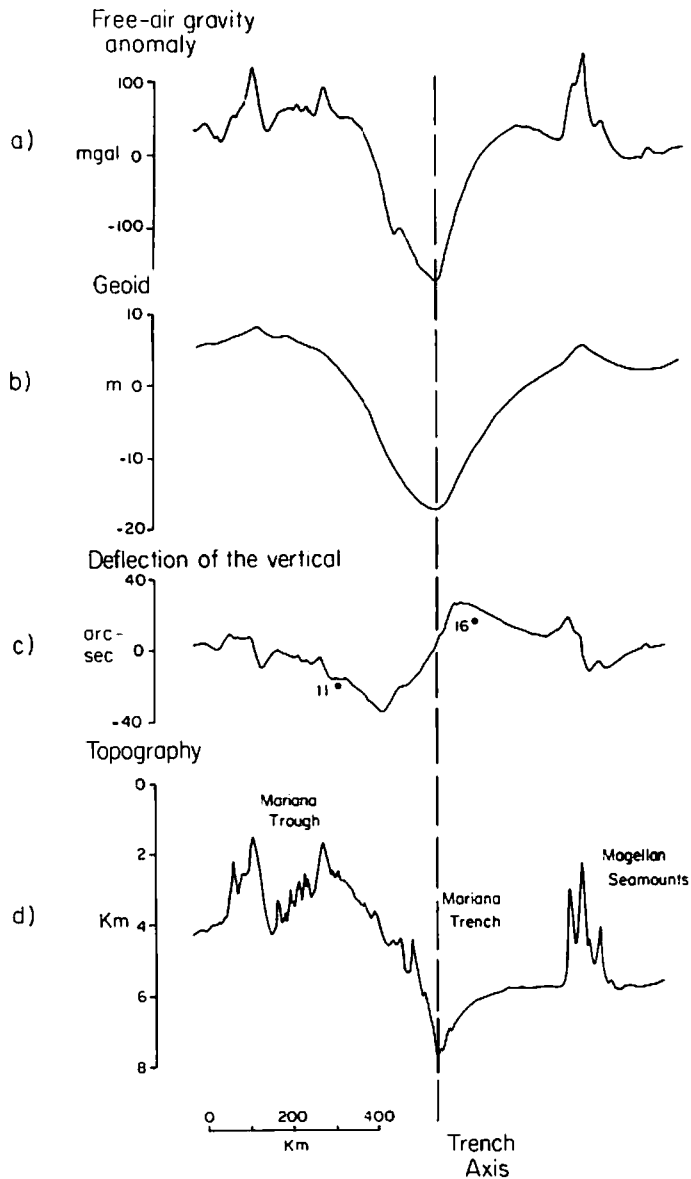


**FIGURE 6.** Free-air gravity anomaly and topography profile AA' of the Mariana trench obtained during R/V Oceanographer cruise 2201B. The geoid and deflection of the vertical profile were computed from the gravity anomaly, assuming two-dimensionality. The solid dots indicate the magnitude of the deflection of the vertical determined at crossovers 11 and 16 from SEASAT altimeter data (Figure 4).

on the intersection of single ascending and descending tracks. The estimates include, however, crossovers of the repeat ascending and descending tracks. In these cases only the mean value of the magnitude and direction of the deflection has been plotted in Figures 4 and 5, since this value probably best represents the gravimetric contribution to the deflection.

In order to test this hypothesis we have compared the altimeter-derived deflections at crossover 25 (Figure 4a) of a single descending track and seven ascending tracks with the nearby crossover of single ascending and descending tracks. Figure 7 shows good qualitative agreement between the mean value of the deflection at estimate 25 and the deflection at nearby crossovers of individual tracks. For example, the mean direction at crossover 25 is within  $5.0^\circ$  to  $11.2^\circ$  of the direction at crossovers 23, 15, and 14. Thus the mean value appears to be a reasonably good estimate of the "reference" gravimetric contribution to the deflection. The actual gravimetric contribution to the deflection at the repeat tracks cannot, however, be reliably determined from SEASAT data because of its relatively short lifetime.

The deflection of the vertical at the crossover points of repeat tracks shows comparatively little scatter about the mean values. This is shown in Figure 8, which summarizes the variations in the deflections at crossover points adjacent to estimate 25. The root mean square (RMS) values of the magnitude and direction of the deflection of the vertical for each crossover point in Figure 8 are  $\pm 1.9$  arc-sec and  $\pm 14.9^\circ$ , respectively.

These variations of the deflections at the crossover of repeat tracks provide a statistical measure of the variability in the deflection estimated at crossovers of individual tracks. Further, they may provide some information on the temporal variability of the deflection.

We illustrate in Figure 9 the variation in deflections at crossover 25 (Figure 4) with time. At this crossover a single descending track, which intersected the crossover on day 218 of 1978, was subsequently crossed by eight ascending tracks that began on day 260 and ended on day 281. Figure 9 shows the estimates of the magnitude  $\gamma$  and direction  $\alpha$  of the deflection for different times during the period from day 260 to day 281. In each case,

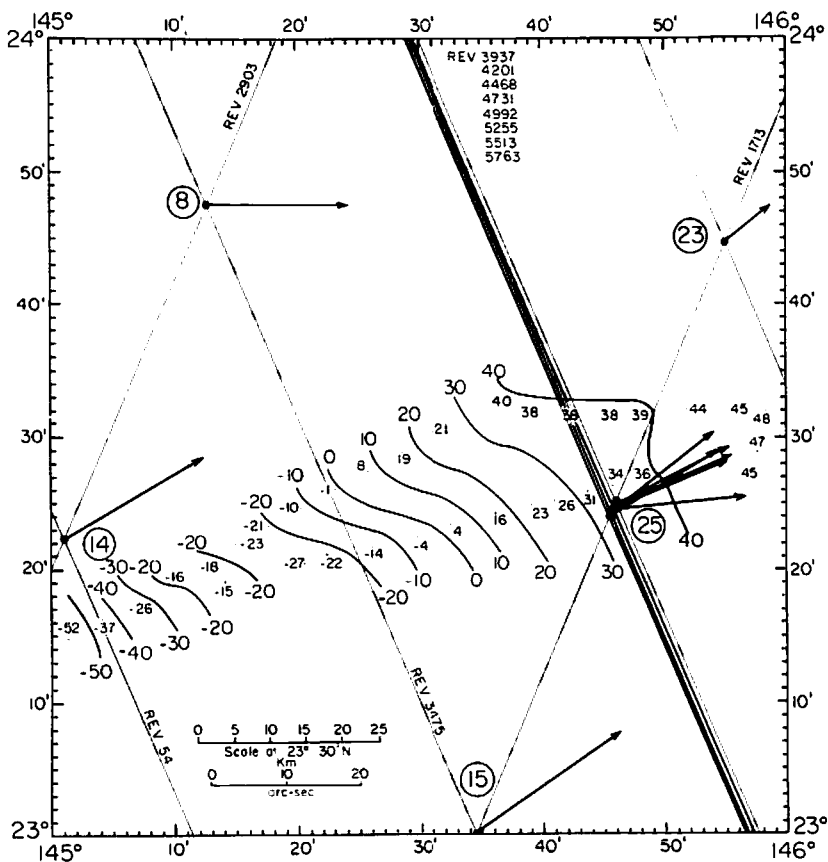
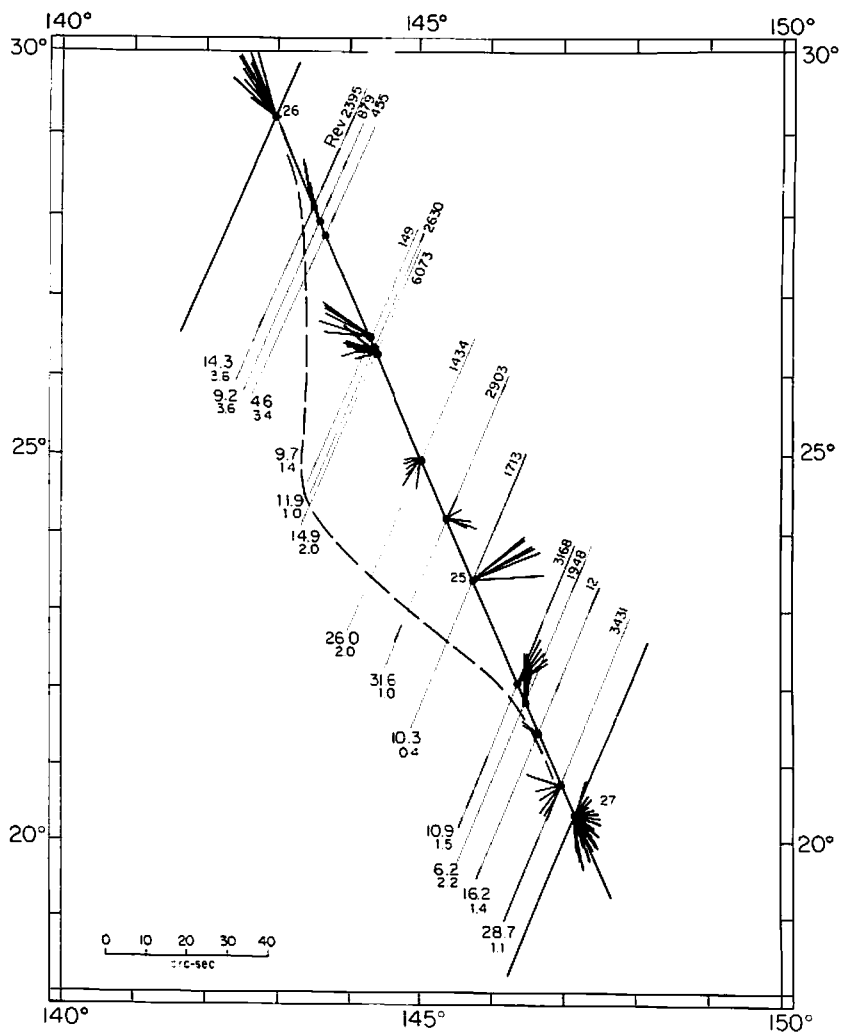
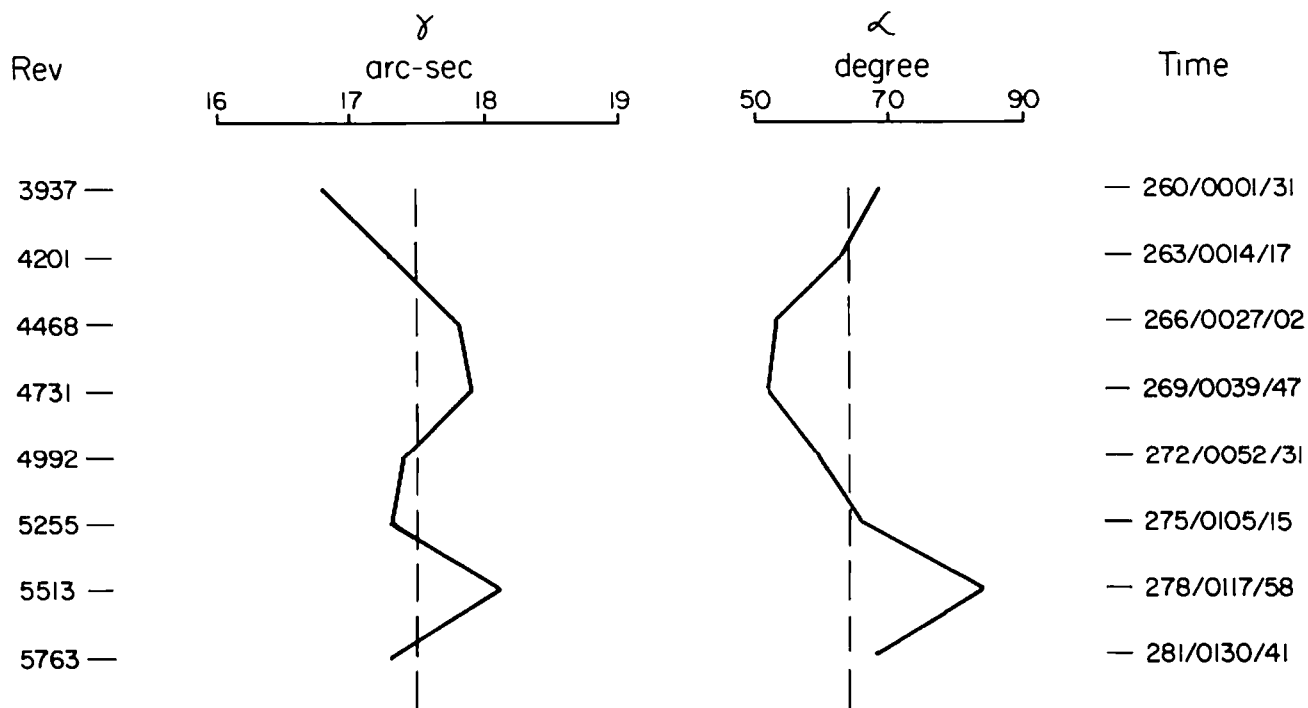


FIGURE 7. Comparison of the deflection of the vertical determined by satellite altimetry with free-air gravity anomaly values for a  $1^\circ$  by  $1^\circ$  "square" over the seaward wall of the Mariana trench. The "square" is centered at latitude  $23^\circ 30' N$  and longitude  $145^\circ 30' W$  and includes estimates 8, 15, 14, 23, and 25 plotted in Figure 4b. Note that only the mean value for the deflection at cross-over 25 is plotted in Figure 4b because there are significant differences in the direction of the deflection at 25. The small numbers indicate actual free-air gravity anomaly values obtained during the R/V Oceanographer cruise 2201 (lower track) and R/V Vema cruise 21 leg 7 (upper track). The gravity anomaly values have been contoured at 10 mgal intervals.



**FIGURE 8.** The deflection of the vertical at the crossovers of ascending tracks 3937 to 5763 with descending tracks between intersections 26 and 27. The deflections obtained at crossover 25 are also plotted in Figures 7 and 9. The lowest numbers on the descending tracks are the RMS values of the magnitude (small numbers) and direction (large numbers) of the deflection of the vertical at each intersection. The RMS value of the magnitude and direction of the deflection of the vertical at all thirteen intersections is  $\pm 1.9$  arc-sec and  $\pm 14.9^\circ$ , respectively. The dashed line indicates the minimum of the free-air gravity anomaly low associated with the Izu-Bonin and Mariana trenches (Figure 5).



**FIGURE 9.** The deflection of the vertical at crossover 25 (Figure 4a) of ascending tracks 3937 to 5763 with descending track 1713. Track 1713 crossed the intersection point on day 218, while tracks 3937 to 5763 crossed it during days 261 and 281. The solid lines are the values of the magnitude  $\gamma$  and direction  $\alpha$  of the deflections. The dashed line is the mean value of  $\gamma$  and  $\alpha$  at the crossover.

the deflection was estimated from the sea-surface slope along the single descending track and the slope along each ascending track.

Figure 9 shows that there is a systematic relationship between the magnitude and direction of the deflection with time at crossover 25. In particular, from day 260 to day 275, as  $\gamma$  increases  $\alpha$  decreases; while from day 275 to day 281, as  $\gamma$  increases  $\alpha$  increases.

The variation in the deflection of the vertical at crossover 25 may be a consequence of instrument noise, oceanic variability, or both. Alternatively, it may result from slight shifts in the position of the crossover point during the repeat tracks that result in a local variation of the gravity field.

In order to examine this hypothesis, we have compared the variations in the deflections at crossover 25 to the available free-air gravity anomaly values in the vicinity of the crossover. Figure 7 shows that a small shift in the position of crossover 25 occurred between days 260 and 281, as the ascending tracks crossed southwest then northwest across the median position of the crossover. The amount of the shift does not exceed 2 km, however, and a nearby ship track indicates that the gravity anomaly gradient in the vicinity of the crossover is only about 1 mgal/km. The effect of this gradient on the deflection at the northwest and southwest crossovers can be calculated by using the gravity anomaly measured on the nearby ship track and Equations (8) and (10). We found that the difference in deflection at the two crossover points caused by the gravity gradient is unlikely to exceed 0.3 arc-sec. In particular, the calculations predict an increase of about 0.3 arc-sec between the crossover of tracks 3937 and 1713 and the crossover of tracks 4731/4992 and 1713, and a decrease in  $\gamma$  by a similar amount between the crossover of tracks 4732/4992 and 1713 and the crossover of tracks 5763 and 1713. These predicted changes in deflections cannot explain either the measured changes (Figure 9) of more than 1 arc-sec between the crossover of tracks 3937 and 1713 and the crossover of tracks 4731/4992 and 1713, or the variations in measured deflections between the crossover of tracks 5763 and 1713 (see Table 2). Further, the gravity anomaly gradient generally follows a northeast-north-

**Table 2**  
 Crossover Analysis at Intersection 25 (Figure 4) of Ascending  
 Tracks 3937 Through 5763 with Descending Track 1713

Ascending Track	Geoid Height		Position of Crossover		Deflection of Vertical	
	Ascending, cm	Descending, cm	Latitude, °N	Longitude, °E	Azimuth, degrees	Magnitude, arc-sec
3937	3716.3	3691.7	23.42	145.77	68.3	16.8
4201	3553.3	3685.1	23.41	145.76	62.9	17.3
4468	3645.7	3678.8	23.41	145.76	52.8	17.8
4731	3457.3	3673.9	23.40	145.76	51.5	17.9
4992	3636.2	3669.7	23.40	145.76	59.7	17.4
5255	3536.6	3673.2	23.40	145.76	65.3	17.3
5513	3689.3	3678.1	23.41	145.76	84.2	18.1
5763	3444.5	3682.9	23.41	145.76	67.6	17.3
Mean	3584.9	3679.2			64.0	17.5
RMS	± 102.7	± 7.2			± 10.3	± 0.4

west trend in the vicinity of crossover 25 and cannot explain the change in direction of the deflections between the crossover of tracks 3937 and 1713 and the crossover of tracks 5763 and 1713.

The most likely cause of the variations in Figure 9 is that they are due to instrument noise, oceanic variability, or both. Brammer and Sailor (1980) have carried out a spectral analysis of SEASAT altimeter data along selected repeat tracks in the Atlantic and Pacific Oceans. They have shown that at wavelengths of about 33 km the SEASAT geoid spectrum intersects a "noise floor" at  $\pm 2.8$  to  $\pm 3.8$  cm (RMS). Brammer and Sailor (1980) suggested that this white noise is associated with instrument noise and oceanic variability. Unfortunately, it is not presently clear how the noise varies as a function of wavelength and whether or not instrument noise or oceanic variability are the principal factors that limit geoidal resolution. If we assume noise levels of  $\pm 2.8$  to  $\pm 3.8$  cm (RMS), for example, then preliminary calculations suggest that most of the variations in Figure 9 can be explained by instrument noise and oceanic variability. However, if oceanic variability rather than instrument noise is the principal factor limiting geoid resolution, as suggested by Brammer and Sailor (1980), then a significant component of the variations in Figure 9 may be caused by oceanic variability.

It was pointed out earlier that the deflection of the vertical is the angle between two normals: one to the geoid and one to the reference ellipsoid. The geoid, however, departs significantly from the ocean surface because of oceanic variability caused, for example, by atmospheric, oceanographic, and tidal effects. Thus, the deflection of the vertical determined from the analysis of data at satellite crossover points would change because of oceanic variability.

We suggest that oceanic variability may cause the changes in the magnitude and direction of the deflection at crossover 25. The systematic relationship between  $\gamma$  and  $\alpha$  shown in Figure 9 suggests rotation of the deflection vector. Figure 9 is therefore a useful way to represent the variability. For example, it would have been difficult to infer this variability from plots of sea-surface heights along each repeat track. As Figure 10 shows, such a plot provides information only on the change of sea-surface heights in the direction of the repeat tracks.

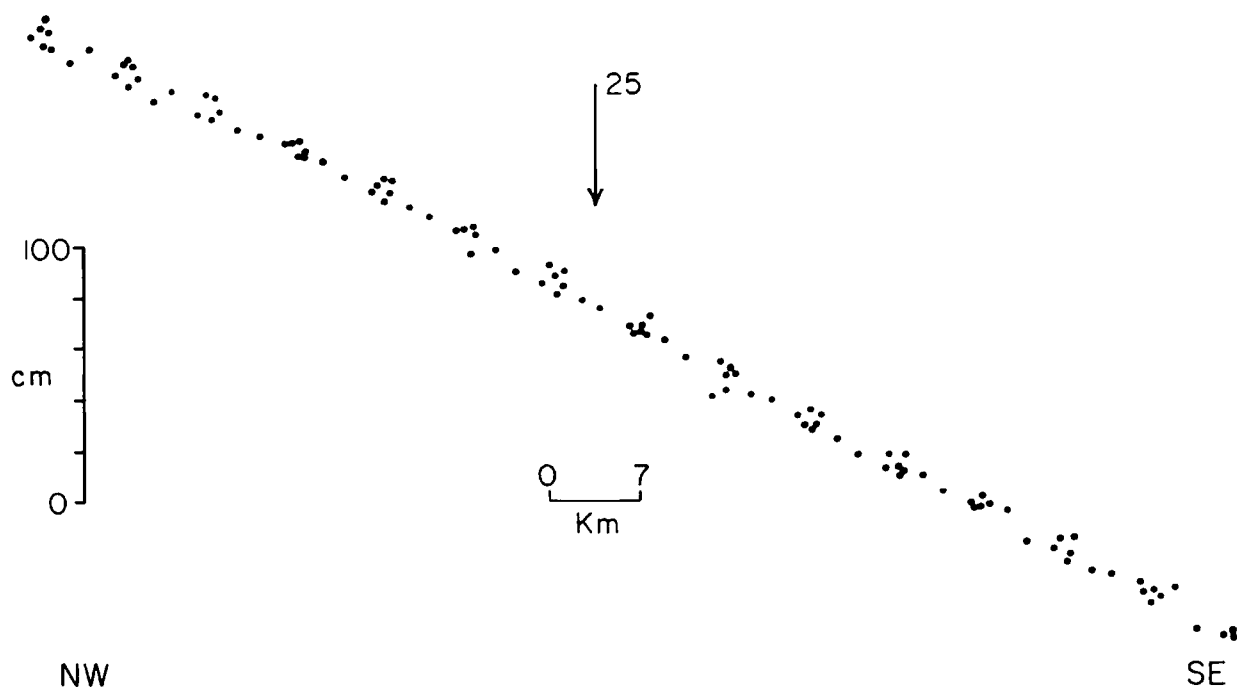


**FIGURE 10.** Sea-surface height profiles measured along the region of the ascending repeat tracks 3937 to 5763 (Figure 9) of crossover 25. The profiles are located between intersections 26 and 27, east of the Izu-Bonin and Mariana trenches. The position of intersection 25 is shown by an arrow above the profiles. Sea-surface heights have had a mean value removed from them and are referred to an ellipsoid with a semimajor axis  $a_r = 6378.145$  km and flattening  $f = 1/298.25$ .

One difficulty with using Figure 9 to directly infer oceanic variability, however, is that sea-surface heights would be expected to vary in the direction of the single descending track *during* the time of the ascending repeat tracks. For example, in the case of crossover 25 there is a forty-two-day gap between the time of the descending track and the time the first of the ascending tracks passes the crossover point. Thus in order to better understand the variability it is necessary to determine deflections at crossovers of repeat tracks where there is a shorter time between descending and ascending tracks.

We have therefore determined deflections at crossovers 26 and 27 in the test area, where there is only a 1.5-day gap between the time the descending track and the first of the ascending tracks pass over a crossover point. Figure 11 shows the variations in deflection at crossover 26 of eight ascending tracks with seven descending tracks. The ascending tracks crossed this point during days 260 and 281, while the descending tracks crossed the point between days 258 and 279. The first of the descending tracks (3817) was crossed by all eight ascending tracks (3937 to 5763), while the last of the descending tracks (5398) was crossed by only two ascending tracks (5513 and 5763). However, because the descending tracks are only about three days apart, a number of independent estimates of the variations of the deflection are obtained at approximately the same point. The fine annotated lines in Figure 11a indicate the deflections obtained by comparing sea-surface slopes measured along each descending track with the slope measured along each subsequent ascending track. The heavy continuous line is the estimated variability, obtained by calculating an average of the deflections for each ascending track.

Figure 11 shows there is a systematic variation in the relationship between  $\gamma$  and  $\alpha$  with time at crossover 26, suggesting variability of the deflection. A useful way to represent this variability is to plot mean values of the magnitude and direction of deflection at a crossover on a spherical plot. Figure 11b shows such an example for crossover 26. In this figure the direction of the deflection  $\alpha$  is plotted in degrees from geographical north (N), and the magnitude of the deflection  $\gamma$  is plotted as a radial

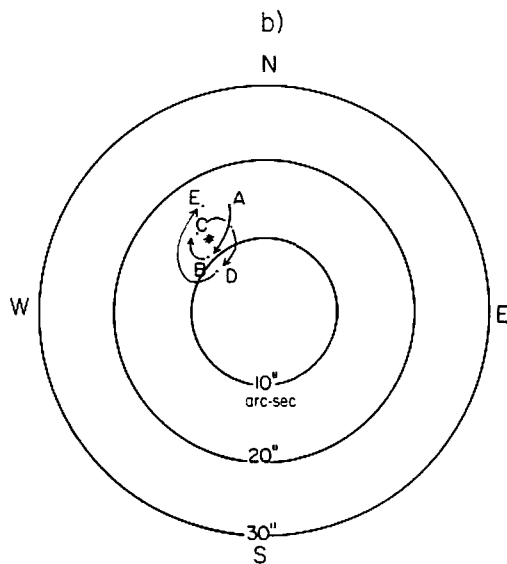
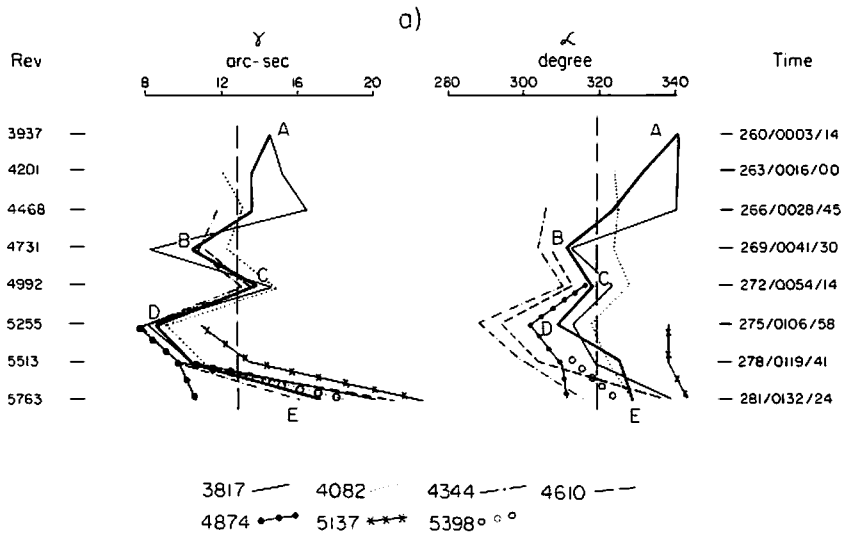


**FIGURE 11.** The deflection of the vertical at intersection 26 of ascending tracks 3937 to 5763 and descending tracks 3817 to 5398. Each determination is based on the sea-surface height of the ascending tracks and the sea-surface height of the preceding descending track. *a.* Plot of magnitude  $\gamma$  and direction  $\alpha$  of the deflection of the vertical. *b.* Plot of the average values of  $\gamma$  and  $\alpha$  at points A to E. The asterisk indicates the overall mean value of the magnitude and direction ( $\bar{\gamma} = 12.7 \pm 3.9$  arc-sec,  $\bar{\alpha} = 319.0 \pm 14.4^\circ$ ) of the deflection. This value is plotted as estimate 26 in Figures 4 and 5.

distance. The arrows, which connect points A to E (Figure 11a), schematically illustrate the rotation of the deflection vector.

The variations in the deflection at crossover 26 (Figure 11) may result in part from slight shifts in the position of the intersection point during the period of the repeat orbits. Individual intersection points (Table 3) generally move in a north-northwest direction, however, across the crossover point. Thus the rapid variations in the deflections at crossover 26 (Figure 11) cannot be attributed only to shifts in the intersection point, because these shifts are slowly varying, essentially in the same direction for each ascending track.

The variability of the deflection vector in Figure 11 may be caused by changes in the local slope of the sea surface over time. In particular, the normal to the sea surface apparently completed nearly two full turns during the time period represented by the ascending and descending tracks. There are two additional problems, however, with interpreting the rotation in terms of temporal changes in sea-surface slopes caused by oceanic variability. First, geostrophic flow in the oceans may contribute to changes in sea-surface slopes, but not to rotation of the deflection vector. Second, the duration of the SEASAT mission was so short that short-term changes (less than about 1.5 days) in

Table 3  
Summary of Possible Contributions to Oceanic Variability

Factor	Range, cm	Length Scale, km	Time Scale, days	Approximate Slope in Sea-Surface Topography, arc-sec
Western Boundary Current	100	100-400	7	0.5-2
Eastern Boundary Current	20	300	10	0.14
Curvature change in major current systems	100	100	7-10	2
Upwelling	20	100	?7	0.4
Eddies	40	100-200	20	0.4-0.8
Spring tides <sup>a</sup> ( $M_2 + S_2$ )	35	400	15	0.15
Neap tides <sup>a</sup> ( $M_2 - S_2$ )	15	400	15	0.07

<sup>a</sup> The values of  $M_2$  and  $S_2$ , the lunar and solar semidiurnal tides, were estimated from cotidal maps of the Pacific Ocean (Parke, 1982).

sea-surface slopes will be aliased in the altimeter-derived deflection data.

We summarize in Table 3 the spatial scales of various oceanic processes that could contribute to long-term changes in sea-surface slopes. The table, which is based on Maul et al. (1980), indicates that oceanographic effects, such as the western boundary currents and eddies, and the spring and neap tides occur with sufficient frequency to be sampled by the altimeter data. The table also shows that the sea-surface slopes associated with oceanographic effects greatly exceed those resulting from the tides. If we assume that the variations in sea-surface slopes are in large part a result of oceanic variability, then it appears from Table 3 that oceanographic effects are too small to fully explain the variability in sea-surface slopes in Figure 11*b*. Other factors, such as the meteorological effects of winds and storms, may therefore also contribute to the altimeter-derived deflections.

### **Tectonic Implications**

The geoid, as determined during the GEOS-3 and SEASAT satellite altimeter missions, has provided useful new constraints on a variety of different tectonic studies in the world's ocean basins. Of particular importance has been the information the geoid has revealed on the long-term mechanical properties of oceanic lithosphere and the driving mechanism of plate tectonics. These two studies are to some extent complementary, of course, since the thermomechanical properties of the plates obscure the geoid anomalies that may be associated with mantle convection.

A number of studies have shown that a significant amount of the energy in the marine geoid can be attributed to the thermomechanical properties of oceanic lithosphere. The majority of these studies (e.g., Roufousse, 1978; Watts, 1979; Cazenave et al., 1980; Lambeck, 1981) have been in the vicinity of seamounts and oceanic islands. These features represent ideal surface loads on the lithospheric plates: they are mainly of volcanic origin, form relatively quickly on the plates, and occur in a variety of tectonic settings.

Geoid anomalies over seamounts and oceanic islands can be

adequately explained by a simple model in which the lithosphere responds to volcanic loads as a thin elastic plate overlying a weak fluid. The model that best fits the data is one in which the flexural rigidity and the equivalent elastic thickness  $T_e$  depend on the age, and hence the thermal structure, of the lithosphere at the time of loading. Seamounts and oceanic islands formed on young lithosphere, on or near a ridge crest, are associated with relatively low-amplitude, short-wavelength geoid anomalies, whereas seamounts formed on old lithosphere are associated with relatively high-amplitude, long-wavelength anomalies. Thus the geoid as measured by satellite altimetry may provide information on the tectonic setting of individual bathymetric features in the world's oceans.

We have previously pointed out (e.g., Watts and Ribe, in press) that the deflection of the vertical depends weakly on the type of flexure model that is assumed at a seamount or oceanic island. Figure 12 shows the deflections that would be expected over a seamount or oceanic island that formed on a continuous elastic plate on or near a ridge crest ( $T_e = 5$  km) or off-ridge ( $T_e = 25$  km). In this figure a positive value indicates a deflection toward the right, whereas a negative value indicates a deflection toward the left. The deflection over the midpoint of the seamount is zero for both values of  $T_e$ . The magnitude of the deflection over the slope of the seamount, however, is a strong function of  $T_e$ . Thus a seamount or oceanic island formed off-ridge is associated with much larger deflections ( $\pm 50$  arc-sec) than a feature formed on-ridge ( $\pm 20$  arc-sec).

The theoretical seamount illustrated in Figure 12 corresponds approximately to the shape of the Hawaiian ridge between Oahu and Molokai in the central Pacific Ocean. Duerksen (1943) determined the deflections on the Hawaiian Islands by using astrogeodetic techniques. In particular, he determined deflections that range up to +34.5 arc-sec on the north coast of Oahu. The model studies (Figure 12), however, indicate a maximum deflection at sea level of  $\pm 35$  arc-sec for the off-ridge model and  $\pm 15$  arc-sec for the on-ridge model. The qualitative agreement between the deflections determined by astrogeodetic techniques and the computed deflections with  $T_e = 25$  km suggest that Oahu

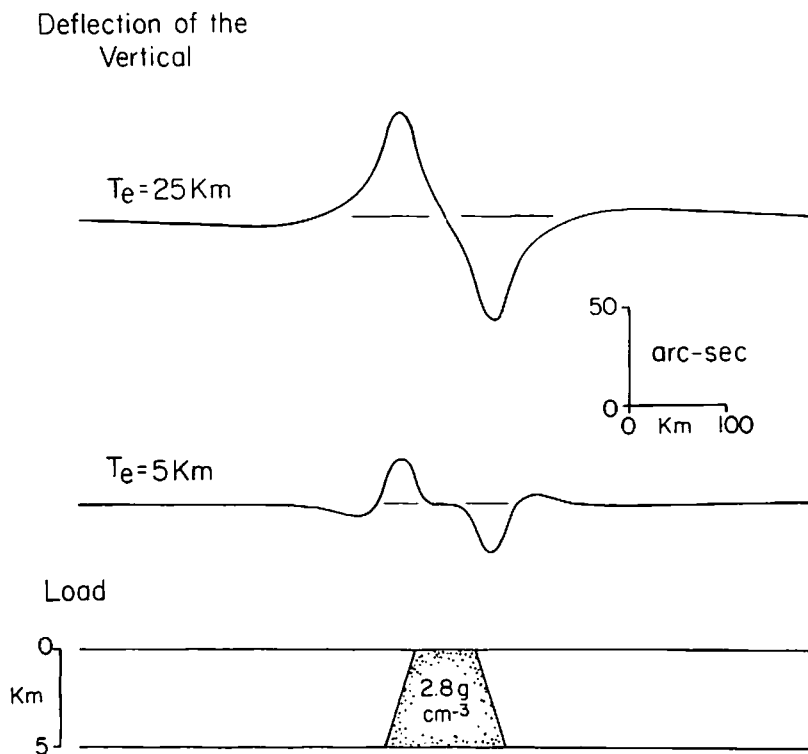


**FIGURE 12.** The deflection of the vertical associated with a two-dimensional seamount load formed on-ridge ( $T_e = 5 \text{ km}$ ) and off-ridge ( $T_e = 25 \text{ km}$ ). The calculations are based on an elastic plate model in which the density of the infill is  $2.8 \text{ g/cm}^3$ , the density of the mantle is  $3.4 \text{ g/cm}^3$ , the density of the material displaced by the load is  $1.03 \text{ g/cm}^3$ , the density of the load is  $2.8 \text{ g/cm}^3$ , and the oceanic crustal thickness before flexure is  $5 \text{ km}$ .

formed on relatively old oceanic lithosphere, an inference that is consistent with the known ages of the island ( $3.1 \pm 1.5 \text{ m.y.}$ ) and the underlying oceanic crust ( $\sim 80 \text{ m.y.}$ ). Thus, the deflection of the vertical in the vicinity of an unsurveyed seamount may provide information on its tectonic setting.

The bathymetry of a large majority of the seamounts and oceanic islands in the Pacific Ocean is highly two-dimensional, however, whereas we assumed in Figure 12 that it is one-dimensional. Further, the maximum widths of these volcanic features are typically much narrower (20 to 110 km) than was assumed in Figure 12.

We show in Figure 13 the deflection of the vertical that would be expected for two isolated seamounts of equal size: one formed on-ridge and one formed off-ridge. These synthetic seamounts are Gaussian in shape and are radially symmetric. Figure 13 shows that a seamount formed on-ridge is associated with relatively small deflections ( $< \pm 10$  arc-sec), whereas the seamount formed off-ridge is associated with relatively large deflections ( $> \pm 15$  arc-sec). Further, deflections associated with the on-ridge seamount point away from the center of the feature and

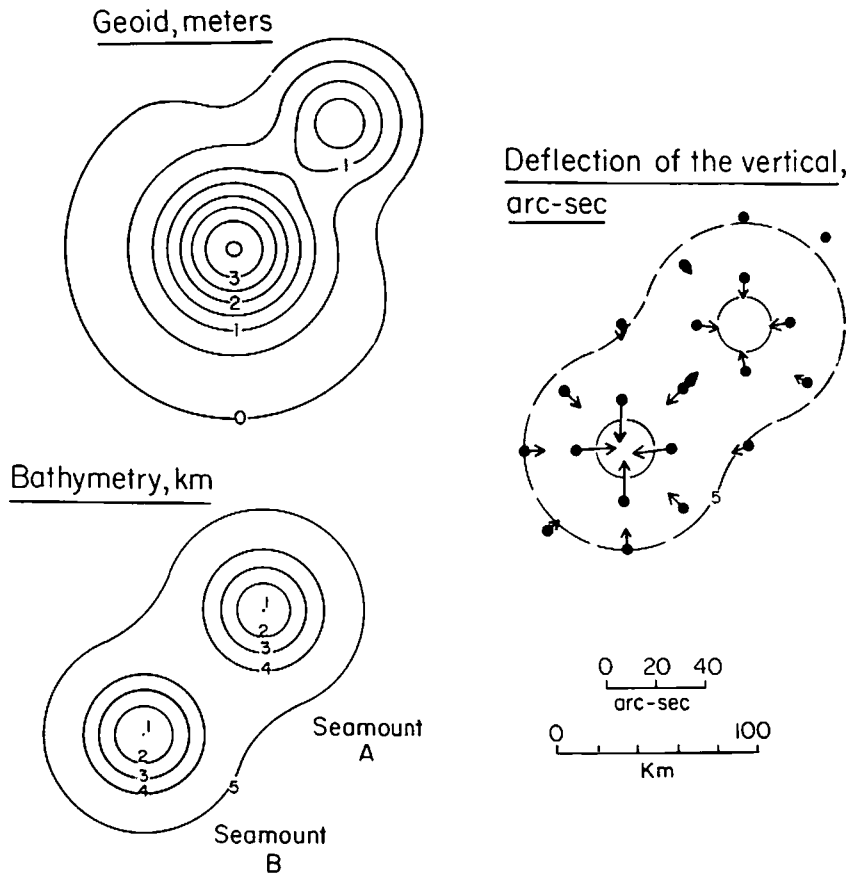


FIGURE 13. The geoid anomaly, deflection of the vertical, and bathymetry for two theoretical gaussian shaped seamounts 4 km high and 100 km apart. The geoid anomaly and deflection have been computed by assuming Seamount A formed on-ridge and Seamount B formed off-ridge.

towards the off-ridge seamount. This is because of the proximity of the on-ridge seamount to the mass excess of the off-ridge seamount. The deflections associated with the off-ridge seamount, however, point away from the on-ridge seamount. We attribute this to the proximity of the off-ridge seamount to the mass deficiency of the flexural depression of the on-ridge seamount. Figure 8 indicates that it should be possible to determine deflections by satellite altimetry to about  $\pm 2$  arc-sec. Thus, Figure 14 implies that it should be possible to use altimeter-derived deflections to determine whether a seamount formed on or near a ridge crest or off-ridge.

In order to test this possibility we have examined deflections in two small areas in the Pacific Ocean, between the Mariana trench and the Hawaiian Islands. The first area includes the northern extremity of the Line Islands ridge, the Cross-Line trend, and the southeastern portion of the Mid-Pacific mountains, while the second area encompasses a large portion of the Magellan Seamounts and the Marcus-Wake guyots. These areas are shown in more detail in Figures 14 and 15. The left-hand side of each figure shows the bathymetry and the distribution of SEASAT tracks. The solid dots are the crossover points for which the deflections of the vertical have been computed. The right-hand sides of Figures 14 and 15 show the deflection of the vertical, with the length and direction of the arrow indicating the magnitude and the direction of the deflection, respectively.

Figures 14 and 15 show that deflections reach magnitudes of up to 25 arc-sec in the vicinity of isolated seamounts and oceanic islands and generally point toward the center of the feature. For example, deflections in the vicinity of A and B (Figure 15) point toward the center of two isolated seamounts in the Magellan Seamounts.

The Magellan Seamounts and Line Islands provinces include seamounts roughly comparable in size, but their associated deflections of the vertical are strikingly different. The Magellan Seamounts are associated with deflections of up to 25 arc-sec (Figure 14), whereas the Line Islands (Figure 15) are associated with deflections of up to 10 arc-sec. There are exceptions to this general relationship. For example, relatively large deflections (of

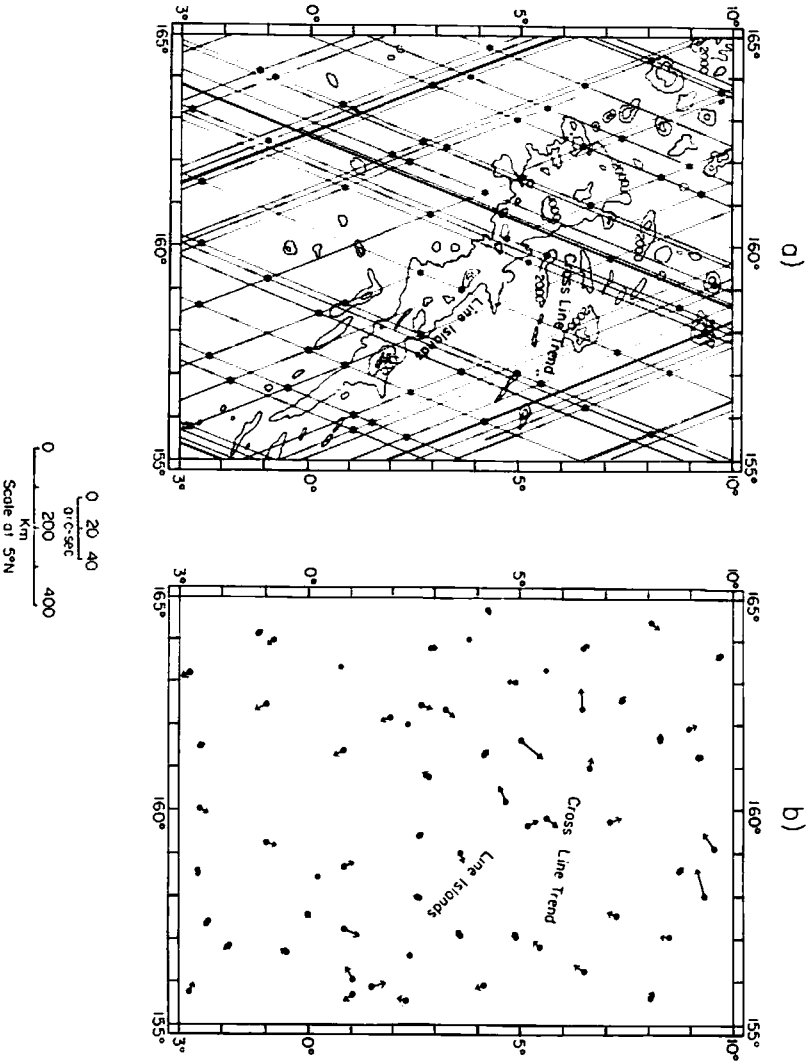
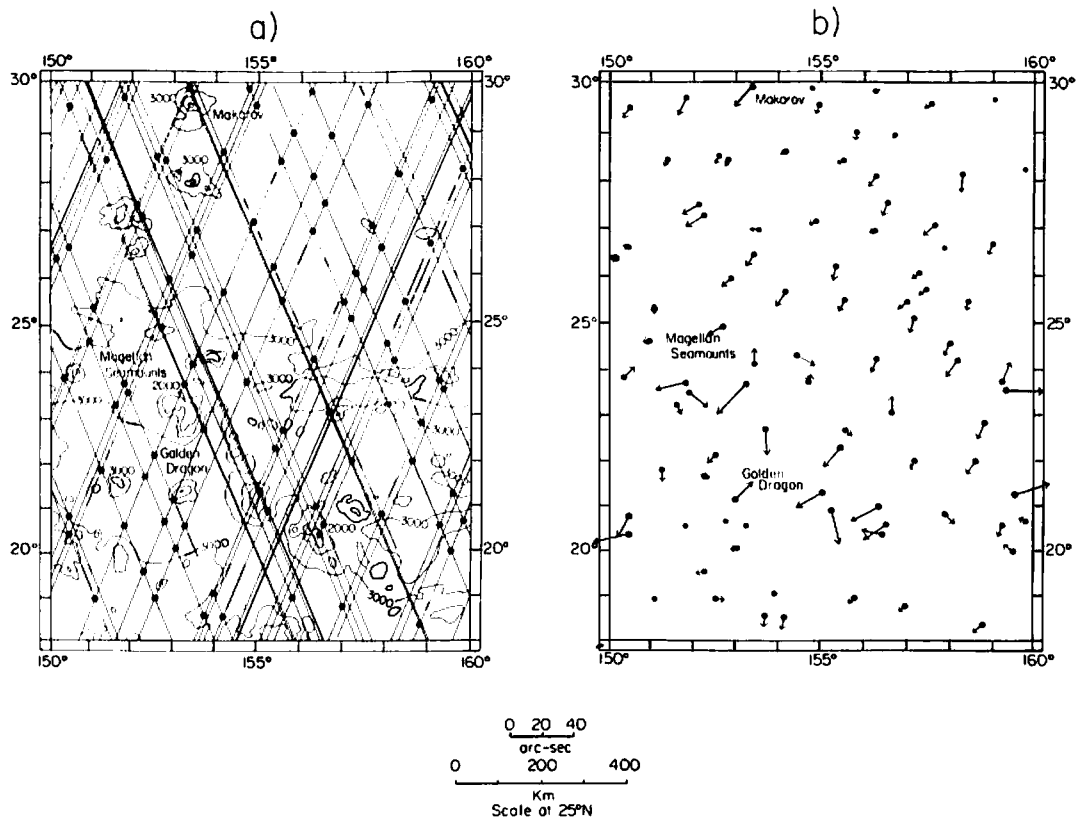


FIGURE 14. SEASAT altimeter tracks, bathymetry, and deflections of the vertical in the vicinity of the Line Islands, central Pacific Ocean. The symbols and bathymetric contour interval are as defined in Figure 4.



**FIGURE 15.** SEASAT altimeter tracks, bathymetry, and deflections of the vertical in the vicinity of the Magellan Seamounts, western Pacific Ocean. The symbols and bathymetric contour interval are as defined in Figure 4.

up to 20 arc-sec) are associated with some seamounts in the Line Islands. These seamounts, however, are associated with the Cross-Line trend, which morphologic and radiometric age dating studies (e.g., Winterer, 1976) suggest are significantly younger in age than the Line Islands ridge.

We interpret the differences in the magnitude of the deflection in the two areas as a result of variations in tectonic setting of seamounts in the two regions. In particular, the large deflections in the Magellan Seamount region suggest they formed on old, strong lithosphere, while the small deflections in the Line Islands region indicate they formed on young, weak lithosphere. These inferences for the tectonic setting of these features is in accord with available geological studies in the region. For example, the results of available dredge hauls (Heezen et al., 1973) suggest that the Magellan Seamounts formed on oceanic lithosphere as old as 50 m.y., while Deep Sea Drilling Project results suggest the age of the Line Islands is not significantly different than the age of the lithosphere on which they formed (Schlanger and Silva, 1981).

The deflections in Figures 14 and 15 cannot all be interpreted in terms of bathymetric features that formed on-ridge or off-ridge. For example, Figure 14 shows a number of deflections of 5 to 10 arc-sec. oriented in a south-southwest direction over relatively smooth floor in the northeast part of the map area. These deflections result in part from the steep geoid gradient that marks the northern boundary of the Philippine Sea–New Guinea geoidal high that is so prominent on total geoid maps of the region (e.g., Watts and Leeds, 1977; Horai, 1982). This gradient is approximately 0.02 m/km and could contribute to regional changes in sea-surface slopes of about 4 arc-sec.

We have interpreted the magnitude of the deflection of the vertical in the vicinity of a seamount in terms of the mechanical properties of the lithosphere and the tectonic setting of the feature. In order to establish this correlation more quantitatively, however, it will be necessary to determine the contribution to the deflections of the actual bathymetric feature in question. Unfortunately, detailed bathymetric surveys of the majority of sea-

mounts in the Magellan Seamounts and Line Islands regions are not yet available.

The computed and measured deflections in Figures 12 to 15 have a number of important implications for isostatic studies and for missile-firing evaluations in the oceans. First, the large differences in deflections between features formed on-ridge and off-ridge should allow deflections determined from altimeter data to be used to estimate the tectonic setting of a bathymetric feature with only rudimentary knowledge of the bathymetry. Second, the large differences in deflections suggest that the range of a projectile is likely to vary according to whether it is launched next to a bathymetric feature formed on-ridge or off-ridge.

Clearly, more detailed data on gravity anomalies and bathymetry must be obtained in oceanic regions in the future if we are to verify and fully evaluate the significance of the deflection of the vertical as determined from altimeter data. Preliminary studies, however, suggest that satellite altimetry provides a promising new way to look at oceanic variability and the tectonic evolution of the world's ocean basins.

## **Conclusions**

We can draw the following conclusions from this study on the determination of the deflection of the vertical by satellite altimetry.

Satellite altimeter data can be used to determine the deflection of the vertical at sea at crossovers of ascending and descending tracks.

The RMS difference in the magnitude and direction of deflections obtained along a SEASAT repeat track in the region of the Izu-Bonin and Mariana trenches is  $\pm 1.9$  arc-sec and  $\pm 10.9^\circ$ , respectively. This variability is most probably a result of instrument noise and oceanic variability.

The deflection of the vertical in the vicinity of the Izu-Bonin and Mariana trenches reaches magnitudes of up to 33 arc-sec and generally points outwards from the axis of the trench. There is generally a good correlation between the direction of the de-

deflection and the direction of the greatest horizontal gravity gradients, except in regions of sparse gravity data.

The deflection at the Izu-Bonin and Mariana trenches is a result of the overall mass deficiency that exists in trench regions compared to that of adjacent island arc and outer rise regions. The modelling of the deflection, however, is complicated by the unknown density structure of these regions.

The deflection of the vertical in the vicinity of seamounts and oceanic islands in the Pacific Ocean reach magnitudes of up to 25 arc-sec and generally point towards the center of these features.

The deflection is a strong function of the flexural rigidity or equivalent elastic thickness of oceanic lithosphere.

The deflection is generally large in the region of the Magellan Seamounts and small in the vicinity of the Line Islands. These differences are attributed to formation of the Magellan Seamounts on stronger, more flexible lithosphere than the Line Islands ridge.

### **Acknowledgments**

We thank R. Bell and four anonymous reviewers for their comments on the manuscript. This work was supported by the Office of Naval Research under contract N00014-80-C-0098, Scope B.

### **References**

- Airy, G. B. 1855. On the computation of the effect of the attraction of mountain masses, as disturbing the apparent astronomical latitude of stations in geodetic surveys. *Phil. Trans. Roy. Soc.* 145: 101–104.
- Brammer, R. F. 1979. Estimation of the ocean geoid near the Blake escarpment using Geos 3 altimetry data. *J. Geophys. Res.* 84: 3843–3852.
- Brammer, R. F., and Sailor, R. V. 1980. Preliminary estimates of the resolution capability of the Seasat Radar Altimeter. *Geophys. Res. Lett.* 7: 193–196.
- Cazenave, A., Lago, B., Dominti, K., and Lambeck, K. 1980. On the response of the ocean lithosphere to seamount loads from GEOS 3 satellite radar altimetry observations. *Geophys. J. R. Astr. Soc.* 63: 233–252.
- Chase, T. E., Menard, W. H., and Mammerickx, J. 1971. Topography of the North Pacific. *IMR Tech. Rept.* Series TR-17.

- Duerksen, J. A. 1943. Gravity anomalies and meridian deflections in Hawaii. *Transactions, Amer. Geophys. Union, Reports and Papers, Geodesy*, 34–39.
- Dutton, C. E. 1882. Physics of the Earth's crust; by the Rev. Osmond Fisher, M.A., F.G.S. *Amer. Jour. Sci.*, third series, 23: 283–290.
- Everest, G. 1842. On the astronomical circles of the grand trigonometrical survey of India, with a description of the methods employed to remedy their defects. *Astron. Soc. Mem.* XII: 141–152.
- Fischer, I. 1979. The effect of the Mid-Atlantic Ridge in terms of gravity anomalies, geoidal undulations, and deflections of the vertical. *Mar. Geod.* 2: 215–217.
- Fischer, I., and Wyatt, P., III. 1974. Deflections of the vertical from bathymetric data. Defense Mapping Agency, Topographic Center, Washington, DC. *International Symposium on Applications of Marine Geodesy*, 1–13.
- Heezen, B. C., et al. 1973. Western Pacific guyots. *Initial Report of the Deep Sea Drilling Project*, Vol. 2. U.S. Government Printing Office, Washington, DC, pp. 653–723.
- Heiskanen, W. O., and Vening Meinesz, F. A. 1958. *The Earth and Its Gravity Field*. McGraw-Hill, New York, 470 pp.
- Horai, K. 1982. A satellite altimetric geoid in the Philippine Sea. *Nature* 299: 117–121.
- Lambeck, K. 1981. Flexure of the ocean lithosphere from island uplift, bathymetry, and geoid height observations: the Society Islands. *Geophys. J. R. Astr. Soc.* 67: 91–114.
- Leitao, C. D., and McGoogan, J. T. 1975. Skylab radar altimeter: short-wavelength perturbations detected in ocean surface profiles. *Science* 186: 1208–1209.
- Lorell, J., Parke, M. E., and Scott, J. F. 1980. *Geophysical data record (GDR) users' handbook*, Jet Propulsion Laboratory, Pasadena, CA, 90 pp.
- McKenzie, D. P., and Bowin, C. 1976. The relationship between bathymetry and gravity in the Atlantic Ocean. *J. Geophys. Res.* 81: 1903–1915.
- Marsh, J. G., and Chang, E. S. 1978. Five-foot detailed gravimetric geoid in the northwestern Atlantic Ocean. *Mar. Geod.* 1: 253–261.
- Maul, G. A., Mourad, A. G., Wilson, P., Shemdin, O. H., Estes, R. H., and Weiffenbach, F. 1980. Report on international symposium on interaction of marine geodesy and ocean dynamics. *Mar. Geod.* 3: 3–25.
- Nagy, D. 1963. Gravimetric deflections of the vertical by digital computer. *Pub. Dom Obs.* 28: 5–71.
- Parke, M. E. 1982. O1, P1, N2 models of the global ocean tide on an elastic earth plus surface potential and spherical harmonic decompositions for M2, S2, and K1. *Mar. Geod.* 6: 35–81.
- Pratt, J. H. 1855. On the attraction of the Himalaya mountains, and of the elevated regions beyond them, upon the plumb-line in India. *Trans. Roy. Soc. Lond. Series (B)*. 53–100.

- Pratt, J. H. 1858. On the deflection of the plumb-line in India, caused by the attraction of the Himalaya mountains and of the elevated regions beyond, and its modification by the compensating effect of a deficiency of matter below the mountain mass. *Trans. Roy. Soc. Lond. Series (B)*, 745–796.
- Rapp, R. H. 1979. GEOS-3 data processing for the recovering of geoid undulations and gravity anomalies. *J. Geophys. Res.* 84: 3784–3792.
- Rice, D. A. 1952. Deflections of the vertical from gravity anomalies. *Bull. Géod.* 25: 285–312.
- Roufousse, M. C. 1978. Interpretation of altimeter data. *Proc. 9th GEOP Conf. An int. symp. on the applications of geodesy to geodynamics*, Dept. Geodetic Sci. Rep., Ohio State Univ. 280: 261–66.
- Sandwell, D. T. 1984. A detailed view of the South Pacific geoid from satellite altimetry. *J. Geophys. Res.* 89: 1089–1104.
- Schlanger, S. O., and Silva, I. P. 1981. Tectonic, volcanic, and paleogeographic implications of redeposited reef faunas of Late Cretaceous and Tertiary age from the Nauru Basin and the Line Islands. *Initial Reports of the Deep Sea Drilling Project*. U.S. Government Printing Office, Washington, DC, 61: 817–827.
- Schutz, B. E., Tapley, B. D., and Shum, C. 1982. Evaluation of the SEASAT altimeter time tag bias. *Jour. Geophys. Res.* 87: 3239–3245.
- Tapley, B. D., Born, G. H., and Parke, M. E. 1982. The SEASAT altimeter data and its accuracy assessment. *J. Geophys. Res.* 87: 3179–3188.
- von Arx, W. S. 1966. Level-surface profiles across the Puerto Rico trench. *Science* 154: 1651–1653.
- Watts, A. B. 1976. Gravity field of the northwest Pacific Ocean basin and its margin: Philippine Sea. *Geol. Soc. Amer. Spec. Map and Chart Series* MC-12.
- Watts, A. B. 1979. On geoid heights derived from GEOS-3 altimeter data along the Hawaiian-Emperor seamount chain. *J. Geophys. Res.* 84: 3817–3826.
- Watts, A. B., Bodine, J. M., and Ribe, N. M. 1980. Observations of flexure and the geological evolution of the Pacific Ocean basin. *Nature* 283: 532–537.
- Watts, A. B., and Leeds, A. R. 1977. Gravimetric geoid in the northwest Pacific Ocean. *Geophys. J. R. Astr. Soc.* 50: 249–278.
- Watts, A. B., and Ribe, N. M. In press. On geoid heights and flexure of the lithosphere at seamounts. *J. Geophys. Res.*
- Winterer, E. L. 1976. Anomalies in the tectonic evolution of the Pacific. *The Geophysics of the Pacific Ocean Basin and Its Margin*, AGU Monograph 19. American Geophysical Union, Washington, DC, 269–278.